

Synthesis and luminescence properties of $\text{La}_2\text{O}_2\text{S}:\text{Eu}^{3+}$ hollow nanofibers derived from $\text{La}_2\text{O}_3:\text{Eu}^{3+}$ hollow nanofibers

FEI BI^{a,*}, JIAQI LI^b, GUANGQING GAI^{a,*}, XIANGTING DONG^{b,*}

^aLaboratory of Building Energy-Saving Technology Engineering, College of Material Science and Engineering, Jilin Jianzhu University, Changchun 130118, China

^bKey Laboratory of Applied Chemistry and Nanotechnology at Universities of Jilin Province, Changchun University of Science and Technology, Changchun 130022, China

$\text{La}_2\text{O}_2\text{S}:\text{Eu}^{3+}$ hollow nanofibers were successfully fabricated by sulfurization of the relevant $\text{La}_2\text{O}_3:\text{Eu}^{3+}$ hollow nanofibers via double-crucible method. The morphology and properties of the products were investigated in detail by X-ray diffraction (XRD), scanning electron microscope (SEM) and fluorescence spectrometer. $\text{La}_2\text{O}_2\text{S}:\text{Eu}^{3+}$ hollow nanofibers were pure hexagonal phase with space group P-3m1 and were hollow-centered structure with the mean diameter of 100.87 ± 12.89 nm. Emission spectra analysis manifested that $\text{La}_2\text{O}_2\text{S}:\text{Eu}^{3+}$ hollow nanofibers emitted red emission at 624 nm attributed to ${}^5\text{D}_0 \rightarrow {}^7\text{F}_2$ energy levels transition of Eu^{3+} ions. CIE analysis demonstrated that the emitting colors of $\text{La}_2\text{O}_2\text{S}:\text{Eu}^{3+}$ hollow nanofibers were located in the yellow and red regions and color-tuned luminescence can be obtained by changing doping concentration of Eu^{3+} ions, which could be applied in the field of optical telecommunication and optoelectronic devices. The possible formation mechanism of $\text{La}_2\text{O}_2\text{S}:\text{Eu}^{3+}$ hollow nanofibers were also proposed.

(Received July 3, 2019; accepted June 16, 2020)

Keywords: Lanthanum oxysulfide, Luminescence, Hollow nanofibers, Electrospinning

1. Introduction

In recent years, nanomaterials have been extensively studied because of their distinctive geometries, novel physical and chemical properties, and potential applications in nanoscale optical and electric devices [1-5]. Among these nanomaterials, nanofiber is a new kind of one-dimensional nanomaterials with special morphology. It has attracted increasing interest of scientists owing to its anisotropy, large length-to-diameter ratio, unique optical, electrical and magnetic performances [6-9]. Research on the fabrication and properties of nanofibers has become one of the popular subjects of study in the realm of nanomaterials.

Electrospinning technology has been extensively explored as a simple and versatile method for forming inorganic superfine nanofibers using polymer/inorganic composite as the precursor [10-13]. The morphology of materials can be controlled by adjusting experimental conditions, such as the viscosity of spinning solution, relative air humidity, the structure of spinneret, spinning voltage, and the distance between the spinneret and the collector. Advantages of this novel process for fabricating 1D nanostructures include, but is not limited to, low cost,

high efficiency and convenient assembly. It has been reported that the nanofibers was successfully synthesized via electrospinning [14-17].

The lanthanide (La-Lu) oxysulfides are known as wide-gap (4.6-4.8 eV) materials suitable for doping ions activation [18-20]. In addition, compared with the lanthanide oxides, oxysulfide is a more efficient phosphor with a broader excitation band. Therefore, the lanthanide oxysulfides become a very important host of inorganic materials which have high potential for applications in various fields, such as color television picture tubes, radiographic imaging, field emission displays, and long-lasting phosphorescence [21, 22]. RE oxysulfides are more biocompatible than RE oxide, may be used as biological probe and label. Some researchers have prepared the $\text{La}_2\text{O}_2\text{S}$ nanomaterials by the sol-gel method and the template methods [23, 24]. Eu^{3+} is a hypersensitive activator to study local symmetry and local environmental. As an efficient red light phosphor, however, Eu^{3+} -doped $\text{La}_2\text{O}_2\text{S}$ nanomaterials were given rather little attention. The reason might be that the $\text{La}_2\text{O}_2\text{S}$ nanomaterials could not be prepared easily. Obtaining bulk $\text{La}_2\text{O}_2\text{S}:\text{Eu}^{3+}$ with good quality is not an easy task.

In this study, pure hexagonal phase $\text{La}_2\text{O}_2\text{S}:\text{Eu}^{3+}$

hollow nanofibers were prepared through calcining the electrospun PVP/[La(NO₃)₃³⁺Eu(NO₃)₃] composite nanofibers, and then La₂O₂S:x%Eu³⁺ [x stands for molar ratio of Eu³⁺ to (La³⁺+Eu³⁺), x=1, 3, 5 and 7] hollow nanofibers were fabricated by sulfurization of La₂O₃:x%Eu³⁺ hollow nanofibers *via* a double-crucible method we newly proposed for the first time. The samples were systematically characterized using modern measurements techniques. A possible formation mechanism of La₂O₂S:Eu³⁺ hollow nanofibers was also presented and some meaningful results were obtained.

2. Experimental sections

2.1. Chemicals

Polyvinyl pyrrolidone (PVP) (K15, Mw=10 000, AR) was bought from Tiantai Chemical Co. Ltd. Yttrium oxide (La₂O₃, 99.99%) and europium oxide (Eu₂O₃, 99.99%) were purchased from Kemiou Chemical Co.,Ltd. N, N-dimethylformamide (DMF, AR) and Sulfur powder (S, AR) were purchased from Sinopharm Chemical Reagent Co. Ltd. Nitric acid (HNO₃, AR) was bought from Beijing Chemical Works. All chemicals were directly used as received without further purification.

2.2. Preparation of PVP/[La(NO₃)₃³⁺Eu(NO₃)₃] composite nanofibers *via* electrospinning

In the typical procedure of preparing La₂O₃:5mol%Eu³⁺ hollow nanofibers, 1.712 g of La₂O₃ and 0.097 g of Eu₂O₃ were dissolved in dilute HNO₃ at elevated temperatures to form about 2.4 g of RE(NO₃)₃·nH₂O (RE=La³⁺ and Eu³⁺). The rare earth nitrates were dissolved in 9.8 g of DMF, and then 7.8 g of PVP was added into the above solution. The solution was magnetically stirred for 10 h to form homogeneous transparent precursor solution. Subsequently, the precursor solution was electrospun at room temperature under a positive high voltage of 16 kV, the distance between the capillary tip and the collector (Aluminium foil) was fixed to 18 cm, and relative humidity was 50%-60%. PVP/[La(NO₃)₃³⁺Eu(NO₃)₃] composite nanofibers were obtained on the collector. Other series of La₂O₃:x%Eu³⁺ (x=1, 3 and 7) hollow nanofibers were prepared by the similar procedure except for different doping molar concentration of Eu³⁺.

2.3. Fabrication of La₂O₂S:Eu³⁺ hollow nanofibers

The above PVP/[La(NO₃)₃³⁺Eu(NO₃)₃] composite nanofibers were calcined at 700 °C for 8 h with a heating rate of 1 °C/min. Then the calcination temperature was decreased to 200 °C at a rate of 1 °C/min. Finally, samples were naturally cooled down to room temperature

and La₂O₃:Eu³⁺ hollow nanofibers were obtained.

2.4. Synthesis of La₂O₂S:Eu³⁺ hollow nanofibers

La₂O₃:Eu³⁺ hollow nanofibers were loaded into a small crucible. A few carbon rods were put into a big crucible, and then the small crucible was placed into the big crucible. Next, some sulphur powders were loaded into the space between the two crucibles, and then the big crucible was covered with its lid. We call this process a double-crucible method. Finally the crucibles were annealed at 800°C for 4 h under argon atmosphere, and then the temperature was decreased to 200°C at a rate of 1 °C/min followed by natural cooling down to ambient temperature. Thus, La₂O₂S:Eu³⁺ hollow nanofibers were obtained.

2.5. Characterization methods

The X-ray diffraction (XRD) measurement was performed using a Rigaku D/max-RA XRD diffractometer with Cu Kα line of 0.15418 nm. The field emission scanning electron microscope (FESEM, XL-30, FEI Company) was used to characterize the morphologies and sizes of the products. The distribution histograms of diameters were drawn by Image-Pro Plus 6.0 and origin 8.5 softwares. The excitation and emission spectra of samples were recorded with a HITACHI F-7000 fluorescence spectrophotometer using a Xe lamp as the excitation source. For luminescent measurements, 0.2 g of each sample was loaded into a standard circular cell (sample cell size: 11 mm in diameter, 1.5 mm in thickness) and compacted into a wafer with the thickness of ca. 1.5 mm.

3. Results and discussion

3.1. Crystal structure

Fig. 1 reveals the XRD patterns of La₂O₂S:Eu³⁺ hollow nanofibers. The XRD analysis result of La₂O₂S:Eu³⁺ hollow nanofibers demonstrates that the characteristic diffraction peaks [2θ=25.6°(002), 28.5°(101), 36.4°(012), 44.7°(110), 47.0°(103), 52.3°(112), 53.9°(021), 59.4°(014), 60.7°(113), 66.9°(023), 72.6°(211), 73.3°(105), 77.3°(204)] of the samples can be easily indexed to those of the pure hexagonal phase with primitive structure of La₂O₂S (PDF#71-2098), and the space group is P-3m1. No peaks of any other phases or impurities are also detected, indicating that crystalline La₂O₂S:Eu³⁺ were acquired *via* sulfurization of crystalline La₂O₃:Eu³⁺.

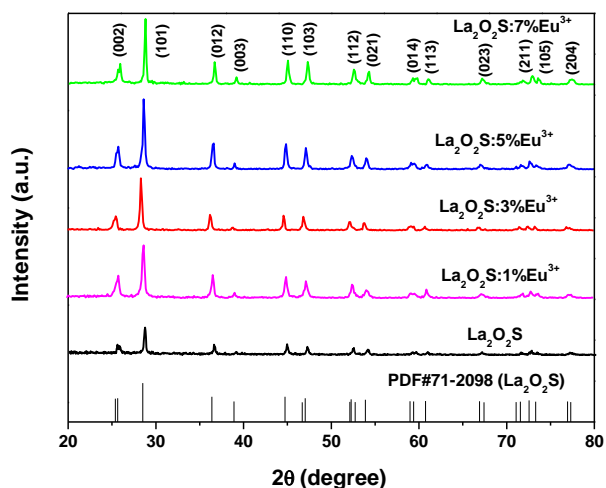


Fig. 1. XRD patterns of $\text{La}_2\text{O}_2\text{S}:x\%\text{Eu}^{3+}$ ($x=1, 3, 5$ and 7) hollow nanofibers (color online)

3.2. Morphology

Fig. 2 shows the representative SEM images of the PVP/[$\text{La}(\text{NO}_3)_3+\text{Eu}(\text{NO}_3)_3$] composite nanofibers, $\text{La}_2\text{O}_3:\text{Eu}^{3+}$ hollow nanofibers and $\text{La}_2\text{O}_2\text{S}:\text{Eu}^{3+}$ hollow nanofibers. From the SEM image of Fig. 2a, it can be noticed that the PVP/[$\text{La}(\text{NO}_3)_3+\text{Eu}(\text{NO}_3)_3$] composite nanofibers have uniform diameter with good dispersivity. Fig. 2b indicates the SEM image of as-prepared $\text{La}_2\text{O}_3:\text{Eu}^{3+}$ hollow nanofibers. It can be clearly seen that the morphology of nanofibers is hollow-centered structure by calcination of the respective electrospun PVP/[$\text{La}(\text{NO}_3)_3+\text{Eu}(\text{NO}_3)_3$] composite nanofibers. After annealing and sulfurization at 800°C , as-formed $\text{La}_2\text{O}_2\text{S}:\text{Eu}^{3+}$ hollow nanofibers have relatively smooth surface, as revealed in Fig. 2c. From Fig. 2c, one can see that the sample exhibits hollow-centered fibrous structure. It reveals that $\text{La}_2\text{O}_2\text{S}:\text{Eu}^{3+}$ hollow nanofibers retain their 1D morphology. From above analyses, we can safely conclude that the sulfurization technique we proposed here can retain the morphology of the precursor nanofibers.

Under the 95 % confidence level, the diameters of PVP/[$\text{La}(\text{NO}_3)_3+\text{Eu}(\text{NO}_3)_3$] composite nanofibers, $\text{La}_2\text{O}_3:\text{Eu}^{3+}$ hollow nanofibers and $\text{La}_2\text{O}_2\text{S}:\text{Eu}^{3+}$ hollow nanofibers analyzed by Shapiro-Wilk method are normal distribution. Distribution histograms of diameters of the samples are indicated in Fig. 3. As seen from Fig. 3, the diameters of PVP/[$\text{La}(\text{NO}_3)_3+\text{Eu}(\text{NO}_3)_3$] composite

nanofibers, $\text{La}_2\text{O}_3:\text{Eu}^{3+}$ hollow nanofibers and $\text{La}_2\text{O}_2\text{S}:\text{Eu}^{3+}$ hollow nanofibers are 452.82 ± 55.43 nm, 147.80 ± 18.52 nm and 100.87 ± 12.89 nm, respectively.

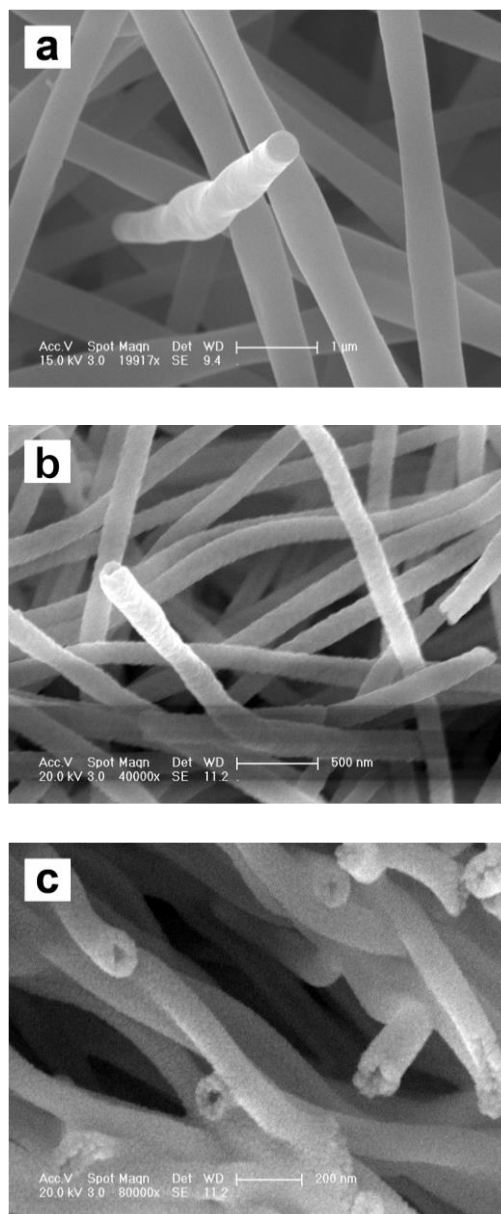


Fig. 2. SEM images of PVP/[$\text{La}(\text{NO}_3)_3+\text{Eu}(\text{NO}_3)_3$] composite nanofibers (a), $\text{La}_2\text{O}_3:\text{Eu}^{3+}$ hollow nanofibers (b) and $\text{La}_2\text{O}_2\text{S}:\text{Eu}^{3+}$ hollow nanofibers (c)

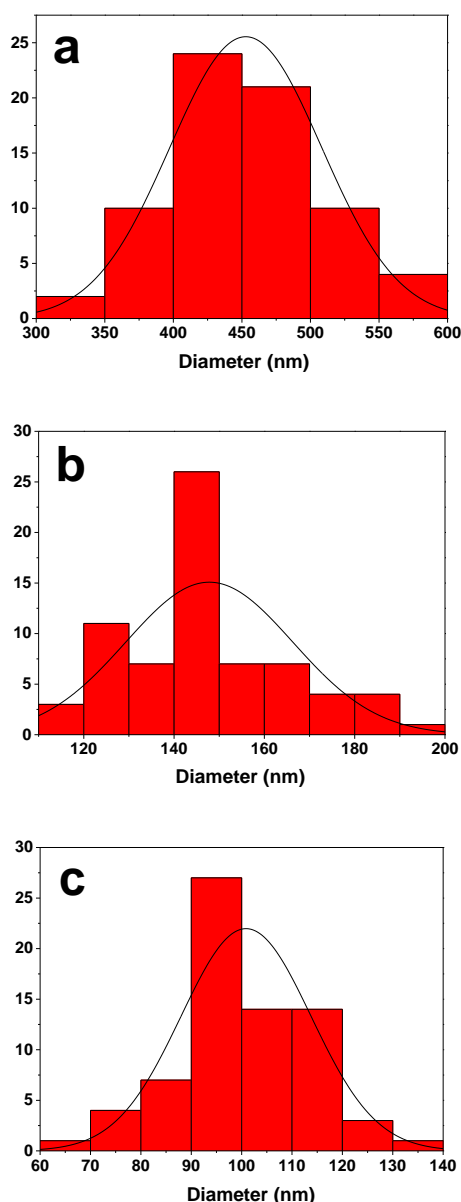


Fig. 3. Distribution histograms of diameters of PVP/[$\text{La}(\text{NO}_3)_3+\text{Eu}(\text{NO}_3)_3$] composite nanofibers (a), $\text{La}_2\text{O}_3:\text{Eu}^{3+}$ hollow nanofibers (b) and $\text{La}_2\text{O}_2\text{S}:\text{Eu}^{3+}$ hollow nanofibers (c) (color online)

3.3. Formation mechanism for $\text{La}_2\text{O}_2\text{S}:\text{Eu}^{3+}$ hollow nanofibers

The formation mechanism for $\text{La}_2\text{O}_2\text{S}:\text{Eu}^{3+}$ hollow nanofibers are proposed on the basis of the above experiment results, as shown in Fig. 4. PVP, $\text{La}(\text{NO}_3)_3$

and $\text{Eu}(\text{NO}_3)_3$ were mixed with DMF to form precursor solution with certain viscosity. Then, PVP/[$\text{La}(\text{NO}_3)_3+\text{Eu}(\text{NO}_3)_3$] composite nanofibers were obtained *via* electrospinning. During calcination process, PVP chain was broken and volatilize. The La^{3+} , Eu^{3+} and NO_3^- ions moved to the surface of the composite fibers with evaporation of solvent DMF. With the increase in calcination temperature, nitrates were decomposed and oxidized to NO_2 , La^{3+} and Eu^{3+} were oxidized to form $\text{La}_2\text{O}_3:\text{Eu}^{3+}$ crystallites, many crystallites were combined into nanoparticles, then some nanoparticles were mutually connected to generate hollow-centered $\text{La}_2\text{O}_3:\text{Eu}^{3+}$ nanofibers. PVP acted as template during the formation of $\text{La}_2\text{O}_3:\text{Eu}^{3+}$ hollow nanofibers. It was found from experiments that the average molecular weight of PVP and content of PVP in the precursor solution played important roles in the formation of $\text{La}_2\text{O}_3:\text{Eu}^{3+}$ hollow nanofibers. Next, $\text{La}_2\text{O}_3:\text{Eu}^{3+}$ hollow nanofibers were sulfurized using sulfur powders as sulfurizing agent. During the process, sulfur powders and $\text{La}_2\text{O}_3:\text{Eu}^{3+}$ hollow nanofibers were separated by the small crucible, which prevented $\text{La}_2\text{O}_3:\text{Eu}^{3+}$ hollow nanofibers from morphology damage. If $\text{La}_2\text{O}_3:\text{Eu}^{3+}$ hollow nanofibers were directly mixed with sulfur powders, melted sulfur will cut the $\text{La}_2\text{O}_3:\text{Eu}^{3+}$ hollow nanofibers into pieces, as a result, the morphology of $\text{La}_2\text{O}_3:\text{Eu}^{3+}$ hollow nanofibers cannot be retained [8, 12, 15]. Carbon rods played an important role in the reduction *via* combination with O_2 to produce CO, which react with oxygen species of $\text{La}_2\text{O}_3:\text{Eu}^{3+}$ to give CO_2 in the heating process. The double-crucible method we proposed here is actually a solid-gas reaction, which has been proved to be an important method, not only can retain the morphology of $\text{La}_2\text{O}_3:\text{Eu}^{3+}$ hollow nanofibers, but also can fabricate $\text{La}_2\text{O}_2\text{S}:\text{Eu}^{3+}$ hollow nanofibers with pure phase at relatively low temperature. Reaction schemes for formation of $\text{La}_2\text{O}_2\text{S}:\text{Eu}^{3+}$ hollow nanofibers proceed as follows:

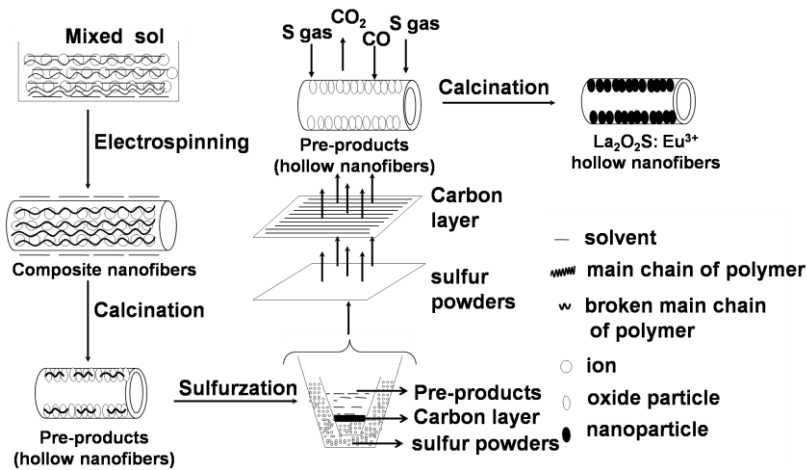
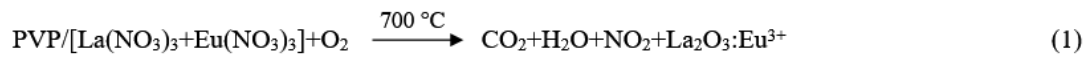


Fig. 4. Formation mechanism of $\text{La}_2\text{O}_2\text{S}:\text{Eu}^{3+}$ hollow nanofibers

3.4. Photoluminescence properties

Fig. 5 shows the excitation and emission spectra of $\text{La}_2\text{O}_3:x\%\text{Eu}^{3+}$ ($x=1, 3, 5$ and 7) hollow nanofibers. Fig.5a showed the excitation spectra of $\text{La}_2\text{O}_3:x\%\text{Eu}^{3+}$ ($x=1, 3, 5$ and 7) hollow nanofibers monitored at 615 nm. The prominent peak at 276 nm was associated with the charge transfer band (CRT) of $\text{O}^{2-}-\text{Eu}^{3+}$. In the longer wavelength region (at 395 nm), the f-f transition peak of Eu^{3+} ions can be observed with very weak intensity compared with those of the CTB. The strongest intensity of excitation spectrum (CTB) was obtained when the doping concentration of Eu^{3+} ion was 5%, as shown in the inset of the Fig. 5a.

Fig. 5b demonstrated that the emission spectrum of the $\text{La}_2\text{O}_3:x\%\text{Eu}^{3+}$ ($x=1, 3, 5$ and 7) hollow nanofibers, when the Eu^{3+} content was greater than 5%, the concentration quenching effect occurred, as shown in the inset of the Fig.5b. At this time, the bond length between Eu^{3+} and O^{2-} became shorter and the mixture of wave function of Eu^{3+} and O^{2-} was enhanced, therefore, the strongest luminescence was at 5%. The emission spectrum was associated with the transitions from the excited level of $^5\text{D}_j$ ($J=0, 1$) to the level of $^7\text{F}_j$ ($J=1, 2$) of Eu^{3+} . The strongest red emission which split into two peaks at 578 nm, 586 nm and 596 nm were ascribed to transition from $^5\text{D}_0 \rightarrow ^7\text{F}_1$ level of Eu^{3+} , which was mainly a magnetic-dipole transition. The peak at 615 nm was ascribed to transition from $^5\text{D}_0 \rightarrow ^7\text{F}_2$ level of Eu^{3+} , which was an electric-dipole transition. The other emission peak at 627 nm was attributed to the electron transition from

$^5\text{D}_0 \rightarrow ^7\text{F}_2$ level of Eu^{3+} .

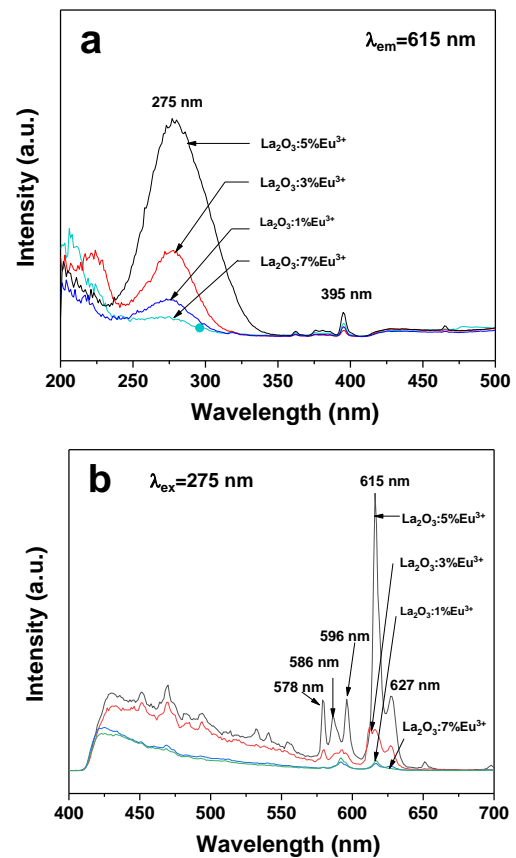


Fig. 5. Excitation (a) and emission (b) spectra of the $\text{La}_2\text{O}_3:x\%\text{Eu}^{3+}$ ($x=1, 3, 5$ and 7) hollow nanofibers (color online)

Fig. 6 shows the excitation (monitored by 624 nm) and emission (excited by 264 nm) spectra of $\text{La}_2\text{O}_2\text{S}:x\%\text{Eu}^{3+}$ ($x=1, 3, 5$ and 7) hollow nanofibers. The excitation spectra (Fig. 6a) exhibits one strong broadband in the range from 200 to 300 nm with a maximum at 264 nm, which is associated to the CT absorption of the 2p orbital of O^{2-} ions to the 4f orbital of Eu^{3+} . And small peak around 324 nm in Fig.6a is attributed to the CT transition from 2p orbital of S^{2-} ions to the 4f orbital of Eu^{3+} ions [18, 24]. The emission spectra of $\text{La}_2\text{O}_2\text{S}:x\%\text{Eu}^{3+}$ ($x=1, 3, 5$ and 7) hollow nanofibers is shown in the Fig. 6b. It is found from Fig.6b that the emission peaks consist of several peaks at 537 nm, 555 nm, 587 nm, 594 nm, 616 nm and 624 nm which originate from the ${}^5\text{D}_1 \rightarrow {}^7\text{F}_2$ and ${}^5\text{D}_0 \rightarrow {}^7\text{F}_2$ energy levels transitions of Eu^{3+} ions, respectively. Among these emission peaks, the red emission at 624 nm attributed to ${}^5\text{D}_0 \rightarrow {}^7\text{F}_2$ energy levels transition of Eu^{3+} ions is the strongest one [24].

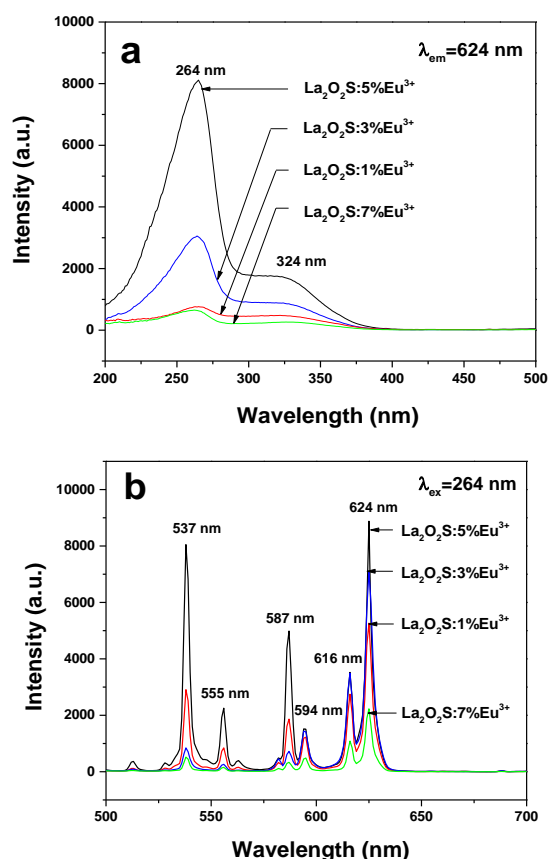


Fig. 6. Excitation (a) and emission (b) spectra of the $\text{La}_2\text{O}_2\text{S}:x\%\text{Eu}^{3+}$ ($x=1, 3, 5$ and 7) hollow nanofibers (color online)

Fig. 6 demonstrates the PL spectra of $\text{La}_2\text{O}_2\text{S}:\text{Eu}^{3+}$ hollow nanofibers with different doping concentrations of Eu^{3+} ions. It is found that the spectral shape and locations of excitation and emission peaks do not vary with the doping concentrations of Eu^{3+} ions for $\text{La}_2\text{O}_2\text{S}:\text{Eu}^{3+}$ hollow nanofibers, but the intensity of excitation and emission peaks for $\text{La}_2\text{O}_2\text{S}:\text{Eu}^{3+}$ hollow nanofibers

strongly depend on the doping concentration of Eu^{3+} ions, and the strongest excitation and emission spectra can be obtained when the doping molar concentration of Eu^{3+} is 5%. Obviously, the luminescence intensity of $\text{La}_2\text{O}_2\text{S}:\text{Eu}^{3+}$ hollow nanofibers increases with the increase of the concentration of Eu^{3+} from the beginning, reaches a maximum value with the Eu^{3+} concentration of 5%, and then decreases with further increase in Eu^{3+} concentration.

PL decay curves of $\text{La}_2\text{O}_2\text{S}:x\%\text{Eu}^{3+}$ ($x=1, 3, 5$ and 7) hollow nanofibers with different concentration of Eu^{3+} are shown in Fig. 7. The samples are excited by 264 nm and monitored at 624 nm. It can be seen that all the curves can be well-fitted into a double-exponential function as $I=A_1\exp(-t/\tau_1)+A_2\exp(-t/\tau_2)$, in which τ_1 and τ_2 are the fast and slow components of the luminescence lifetimes, A_1 and A_2 are the fitting parameters^[25]. With the help of the software Origin 8.5, the values of A_1 , A_2 , and τ_1 , τ_2 can be obtained. The average lifetime of $\text{La}_2\text{O}_2\text{S}:x\%\text{Eu}^{3+}$ ($x=1, 3, 5$ and 7) hollow nanofibers are 0.782 ms, 0.827 ms, 0.935 ms and 0.618 ms, respectively, which were calculated by the formula $\tau=(A_1\tau_1^2+A_2\tau_2^2)/(A_1\tau_1+A_2\tau_2)$ [26].

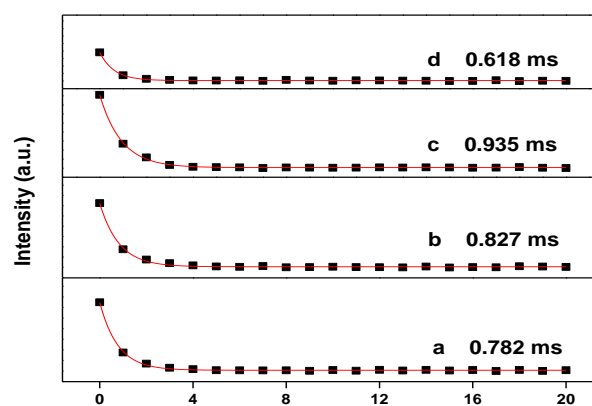


Fig. 7. Luminescence decay curves of $\text{La}_2\text{O}_2\text{S}:x\%\text{Eu}^{3+}$ ($x=1, 3, 5$ and 7) hollow nanofibers (color online)

3.5. CIE analysis

Generally, color is represented by the Commission Internationale de L'Eclairage (CIE) chromaticity coordinates and color ratios. The chromaticity coordinates and color ratios have been calculated from the emission spectra by the method described in previous report[10, 27]. For the $\text{La}_2\text{O}_2\text{S}:x\%\text{Eu}^{3+}$ ($x=1, 3, 5$ and 7) hollow nanofibers, the chromaticity coordinates (X, Y) are determined to be (0.4991, 0.4937), (0.5495, 0.4451), (0.5890, 0.4105) and (0.6221, 0.3747), respectively. Remarkably, the emission colors of $\text{La}_2\text{O}_2\text{S}:x\%\text{Eu}^{3+}$ ($x=1, 3, 5$ and 7) hollow nanofibers shift from yellow to red along with the variation of concentrations of Eu^{3+} , as shown in Fig. 8. These results indicate that the color emissions can be tuned by changing the concentration of doping activator ions. These as-obtained nanostructures could show merits of red emissions, which is considered to

be a promising candidate for application in LEDs [11, 28].

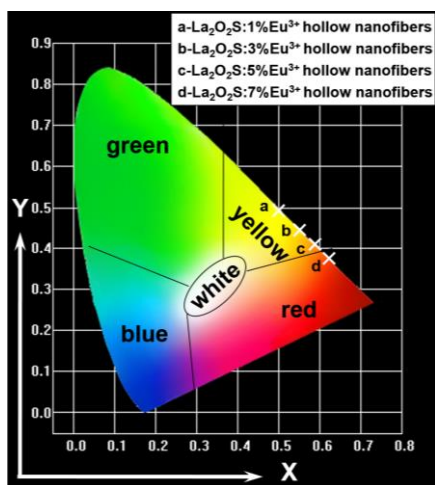


Fig. 8. CIE chromaticity coordinates diagram of $\text{La}_2\text{O}_2\text{S}:x\%\text{Eu}^{3+}$ ($x=1, 3, 5$ and 7) hollow nanofibers (color online)

4. Conclusions

In summary, pure hexagonal phase $\text{La}_2\text{O}_2\text{S}:\text{Eu}^{3+}$ hollow nanofibers with space group P-3m1 were fabricated *via* sulfurization of the $\text{La}_2\text{O}_3:\text{Eu}^{3+}$ hollow nanofibers. The morphology of $\text{La}_2\text{O}_2\text{S}:\text{Eu}^{3+}$ hollow nanofibers can be inherited from $\text{La}_2\text{O}_3:\text{Eu}^{3+}$ hollow nanofibers under the sulfurization circumstance *via* a double-crucible method we newly proposed. The diameters of $\text{La}_2\text{O}_2\text{S}:\text{Eu}^{3+}$ hollow nanofibers analyzed by Shapiro-Wilk method are normal distribution and are 100.87 ± 12.89 nm. Emission spectra analysis manifested that $\text{La}_2\text{O}_2\text{S}:\text{Eu}^{3+}$ hollow nanofibers emitted red emission at 624 nm attributed to ${}^5\text{D}_0 \rightarrow {}^7\text{F}_2$ energy levels transition of Eu^{3+} ions. The double-crucible method we proposed here is of great importance. This technique can be employed to fabrication of other pure-phase rare earth oxysulfide nanomaterials with various morphologies.

Acknowledgements

This work was financially supported by the National Natural Science Foundation of China (NSFC 50972020, 51072026), Ph.D. Programs Foundation of the Ministry of Education of China (20102216110002, 20112216120003), the Science and Technology Development Planning Project of Jilin Province (Grant Nos. 20070402, 20060504), Key Research Project of Science and Technology of Ministry of Education of China (Grant No. 207026), the Science and Technology Research Project of the Education Department of Jilin Province during the thirteenth five-year plan period (Grant No. JJKH20180580KJ, JJKH20180582KJ) and the Scientific Development Program of Jilin Province (Grant No. 20170520152JH).

References

- [1] Y. T. Geng, P. Zhang, Q. T. Wang, Y. X. Liu, K. Pan, *J. Mater. Chem. B* **5**, 5390 (2017).
- [2] J. Zhang, X. B. Hou, Z. Y. Pang, Y. B. Cai, H. M. Zhou, P. F. Lv, Q. F. Wei, *Ceram. Int.* **43**, 15911 (2017).
- [3] N. Lv, Z. G. Wang, W. Z. Bi, G. M. Li, J. L. Zhang, J. Z. Ni, *J. Mater. Chem. B* **4**, 4402 (2016).
- [4] C. Luo, X. X. Wang, J. Q. Wang, K. Pan, *Compos. Sci. Technol.* **133**, 97 (2016).
- [5] X. Xi, Q. L. Ma, W. S. Yu, X. T. Dong, D. Li, W. S. Yu, J. X. Wang, G. X. Liu, *Chem. Plus Chem.* **83**, 108(2018).
- [6] D. Li, Q. L. Ma, Y. Song, X. Xi, X. T. Dong, W. S. Yu, J. X. Wang, G. X. Liu, *J. Am. Ceram. Soc.* **100**, 2034 (2017).
- [7] M. Gao, X. F. Lu, M. Q. Chi, S. H. Chen, C. Wang, *Inorg. Chem. Front.* **4**, 1862 (2017).
- [8] M. K. Liu, Y. F. Du, Y. E. Miao, Q. W. Ding, S. X. He, W. W. Tjiu, J. S. Pan, T. X. Liu, *Nanoscale* **7**, 1037 (2015).
- [9] Y. C. Chou, C. L. Shao, X. H. Li, C. Y. Su, H. C. Xu, M. Y. Zhang, P. Zhang, X. Zhang, Y. C. Liu, *Appl. Surf. Sci.* **285**, 509 (2013).
- [10] F. Bi, X. T. Dong, J. X. Wang, G. X. Liu, *Luminescence* **30**, 751 (2015).
- [11] W. W. Ma, W. S. Yu, X. T. Dong, J. X. Wang, G. X. Liu, *Luminescence* **29**, 908 (2014).
- [12] B. Dong, Z. C. Li, Z. Y. Li, X. R. Xu, M. X. Song, W. Zheng, C. Wang, S. S. Al-Deyab, M. El-Newehy, *J. Am. Ceram. Soc.* **93**, 3587 (2010).
- [13] Y. Wang, H. B. Huang, J. X. Gao, G. Y. Lu, Y. Zhao, Y. Xu, L. Jiang, *J. Mater. Chem. A* **2**, 12442 (2014).
- [14] N. Lv, J. L. Zhang, G. M. Li, X. Wang, J. Z. Ni, *J. Phys. Chem. C* **121**, 11926 (2017).
- [15] D. Li, Q. L. Ma, X. Xi, X. T. Dong, W. S. Yu, J. X. Wang, G. X. Liu, *Chem. Eng. J* **309**, 230 (2017).
- [16] C. X. Zheng, D. Li, Q. L. Ma, Y. Song, X. T. Dong, X. L. Wang, W. S. Yu, J. X. Wang, G. X. Liu, *Chem. Eng. J.* **310**, 91 (2017).
- [17] S. L. Chen, H. Q. Hou, F. Harnisch, S. A. Patil, *Energy Environ. Sci.* **4**, 1417 (2011).
- [18] L. Y. Yang, J. X. Wang, X. T. Dong, G. X. Liu, W. S. Yu, *J. Mater. Sci.* **48**, 644 (2013).
- [19] G. D. Liu, Q. H. Zhang, H. Z. Wang, Y. G. Li, *Sci. Eng. B* **177**, 316 (2012).
- [20] M. Pokhrel, A. K. Gangadharan, D. K. Sardar, *Lett.* **99**, 86 (2013).
- [21] J. J. Oh, B. K. Jin, W. J. Chung, D. W. Shin, Y. G. Choi, *Phys.* **11**, 15 (2011).
- [22] Y. M. Yang, C. Mi, F. Yu, X. Y. Su, C. F. Guo, G. Li, J. Zhang, L. L. Liu, Y. Z. Liu, X. D. Li, *Ceram. Int.* **40**, 9875 (2014).

- [23] N. T. Lau, M. Fang, C. K. Chan, *Catal. B Environ.* **79**, 110 (2008).
- [24] S. V. Yap, R. M. Ranson, W. M. Cranton, D. C. Koutsogeorgis, G. B. Hix, *Lumin.* **129**, 416 (2009).
- [25] C. K. Chang, W. Li, X. J. Huang, Z. Y. Wang, X. Chen, X. Qian, R. J. Guo, Y. L. Ding, D. L. Mao, *Lumin.* **130**, 347 (2010).
- [26] N. Niu, P. P. Yang, W. X. Wang, F. He, S. L. Gai, D. Wang, J. Lin. *Bull.* **46**, 333 (2011).
- [27] D. Li, X. T. Dong, W. S. Yu, J. X. Wang, G. X. Liu, *J. Nanopart. Res.* **15**, 1704 (2013).
- [28] Q. L. Kong, J. X. Wang, X. T. Dong, W. S. Yu, G. X. Liu, *J. Mater. Sci. Mater. Electron.* **24**, 4745 (2013).

* Corresponding author: bifei1224@163.com;
gaigq@163.com;
dongxiangting888@163.com